ARTICLES
PUBLISHED ONLINE: 25 SEPTEMBER 2011 | DOI: 10.1038/NCHEM.1154
nature chemistry

Ultrafast energy flow in the wake of solution-phase bimolecular reactions

David R. Glowacki*, Rebecca A. Rose, Stuart J. Greaves, Andrew J. Orr-Ewing and Jeremy N. Harvey*

Vibrational energy flow into reactants, and out of products, plays a key role in chemical reactivity, so understanding the microscopic detail of the pathways and rates associated with this phenomenon is of considerable interest. Here, we use molecular dynamics simulations to model the vibrational relaxation that occurs during the reaction CN + c-C_6H_{12} → HCN + c-C_6H_{11} in CH_2Cl_2, which produces vibrationally hot HCN. The calculations reproduce the observed energy distribution, and show that HCN relaxation follows multiple timescales. Initial rapid decay occurs through energy transfer to the cyclohexyl co-product within the solvent cage, and slower relaxation follows once the products diffuse apart. Re-analysis of the ultrafast experimental data also provides evidence for the dual timescales. These results, which represent a formal violation of conventional linear response theory, provide a detailed picture of the interplay between fluctuations in organic solvent structure and thermal solution-phase chemistry.

Nearly all chemical reactions involve some degree of vibrational energy transfer[1]. Because typical bond strengths are on the order of tens of kcal per mole, surmounting the energy barriers associated with bond breaking and forming at ambient temperatures requires the localization of significant amounts of energy in a particular vibrational mode. Set against this requirement is the fact that equilibrium statistical mechanics tells us that energy is statistically randomized in all of the states of the system at long times. Thus, understanding the origins and timescales of non-equilibrium energy localization for condensed phase systems with high state densities remains a critical issue in our attempts to develop predictive models of condensed phase chemical reactivity.

The predominant model guiding our understanding of condensed phase non-equilibrium dynamics is linear response theory (LRT)[2], which arises from the fluctuation–dissipation theorem, and amounts to a statement that the relaxation of a system following spontaneous fluctuations from equilibrium is indistinguishable from the relaxation that follows from external preparation of a non-equilibrium system[3]. Despite a few exceptions[4–10], LRT provides a robust framework for understanding relaxation to equilibrium within liquids.

In this Article, we investigate the vibrational relaxation of HCN formed through a bimolecular H abstraction reaction in CH_2Cl_2 solvent, the products of which are illustrated in Fig. 1:

$$CN + c\text{-}C_6H_{12} \rightarrow HCN + c\text{-}C_6H_{11} \qquad (R1)$$

The energies involved in reaction (R1) are characteristic of typical thermal reaction energies, and well within a regime where one might expect relaxation of the vibrationally excited nascent HCN to follow LRT. However, as we will show, the HCN experiences ultrafast changes in the structure of its environment following reaction (R1). This results in multiple LRT relaxation regimes for HCN, which must be properly accounted for to adequately describe our theoretical and experimental observations over the range of post-reaction timescales. Although examples of nonlinear responses have been highlighted for solvation dynamics[4,7,9], electron transfer[6,8] and photochemistry[5,10], this study is the first time (to our knowledge) that such results have been shown for the case of a thermal chemical reaction involving an atomic rearrangement.

Results

Linear response interpretation of the experiments. It has been known for some time that gas-phase abstraction reactions of CN with alkanes, such as reaction (R1), yield HCN that is vibrationally excited in both its CH stretching (00*n*) and HCN bending (0*n*0) modes[11–14], where the numbers in parentheses represent the respective vibrational quantum number of the CN stretch, HCN bend and CH stretch (*n* denotes a range of quantum numbers). In recently published experimental and

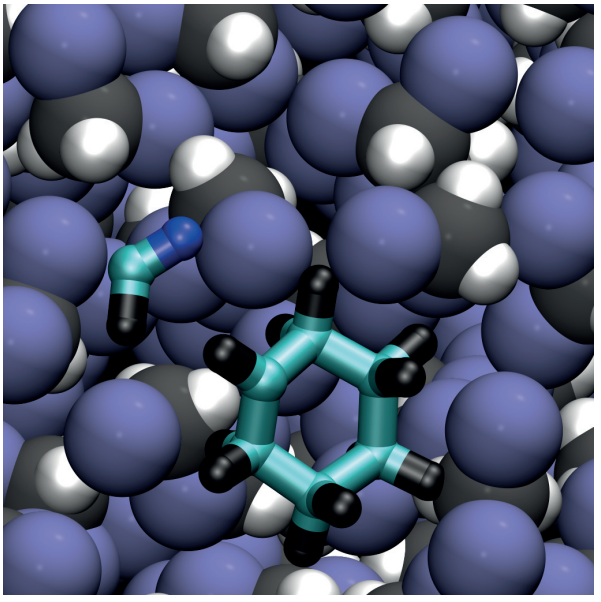

Figure 1 | MD snapshot of the products from reaction (R1). The HCN + c-C_6H_{11} products are displayed such that cyan, black and blue represent carbon, hydrogen and nitrogen, respectively. The products are shown within a CH_2Cl_2 solvent cavity (grey, carbon; violet, chlorine; white, hydrogen).

School of Chemistry, University of Bristol, Bristol BS8 1TS, UK. *e-mail: david.r.glowacki@bristol.ac.uk; Jeremy.Harvey@bristol.ac.uk

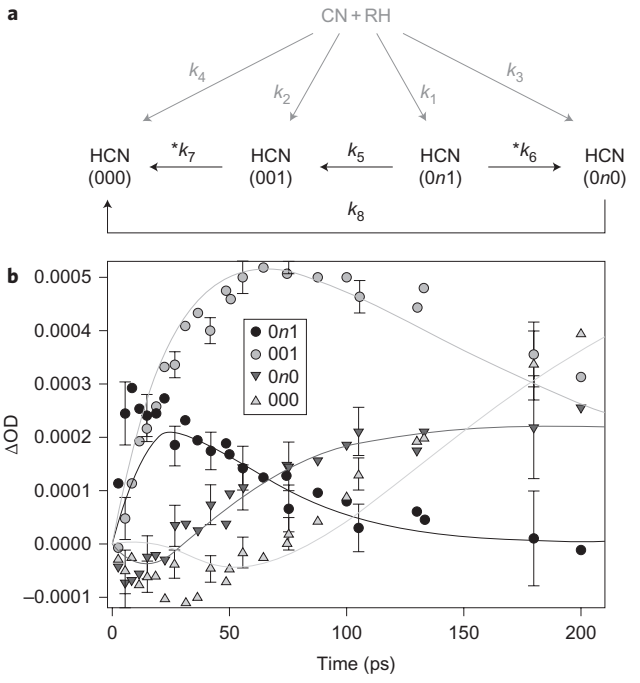

Figure 2 | Simple kinetic model used to rationalize experimentally measured time profiles. a, This model implicitly assumes LRT; that is, HCN relaxation following reaction (R1) is identical to that which occurs in an infrared pump–probe experiment. The asterisk denotes that the fit parameters were not floated, but fixed to experimental infrared pump–probe measurements. **b**, Representative experimental trace showing the changes in optical density (OD) for HCN (0*n*0), (001), (0*n*1) and (000). Representative error bars for individual data points are shown, obtained as ±2 s.d. from least-squares fitting of Gaussian profiles to the measured spectral band intensities[16]. The solid lines show the fit obtained using the kinetic model shown in **a**. The figure shows the poor agreement between model and data at times less than 50 ps.

theoretical work[15,16], CN radicals were generated through ICN photolysis, and the time profile of the vibrational state populations of the nascent HCN generated in reaction (R1) was monitored using ultrafast infrared lasers. The results showed significant HCN vibrational excitation. Gas- and solution-phase molecular dynamics (MD) simulations suggest that the product energy deposition into HCN for reaction (R1) in a CH_2Cl_2 solvent at short times is nearly identical; that is, the product energy specificity is preserved in the corresponding solution-phase reaction following passage over the abstraction transition state (TS)[15]. At longer times, however, the gas-phase and solution-phase results differ—whereas the energy of the HCN and *c*-C_6H_{11} co-products is conserved in the gas phase, it relaxes to thermal equilibrium in solution.

In our previous work, the experimental time traces obtained from reaction (R1) were fit using the kinetic model in Fig. 2a, in which the HCN(0*n*1) and HCN(001) relaxation rates were constrained to the experimentally measured k_6 and k_7 decay rates observed from ultrafast pump–probe experiments of vibrationally excited HCN relaxing in CH_2Cl_2 solvent with 1 M *c*-C_6H_{12}. This model implicitly assumes that HCN vibrational relaxation follows standard time-independent linear response theory; that is, the rate of relaxation of HCN to equilibrium is independent of the means through which it was initially prepared, whether via laser pulse or by reaction (R1). Although the kinetic model in Fig. 2a gives good fits to the experimentally observed changes in optical density (OD) at long times, Fig. 2b shows that the fits are less satisfactory at short times, where the negative ODs indicate that the magnitudes of the HCN(000) and HCN(0*n*0) population inversions are underestimated.

One possible explanation for why the model in Fig. 2a underestimates the degree of population inversion at short times is that HCN (002) is formed as well as the nascent HCN(001). However, fitting the data using a numerical integration scheme that includes this channel requires that relaxation from HCN(002) into HCN(001) is at least an order of magnitude faster than the (001) relaxation, and that more than 50% of the HCN produced in reaction (R1) is in the (002) state. These conclusions are at odds with (i) results obtained from our MD simulations, which show that the energy relaxation timescales of (001) ← (002) and (000) ← (001) are very similar (Supplementary Fig. S1), and (ii) our experiments, which suggest an upper limit of 10% for the HCN (002) yield[16].

Non-equilibrium MD simulations: mapping energy flow. Further insight into the experimental results and the origin of the short-time disagreement shown in Fig. 2b was obtained by carrying out a number of MD simulations in a periodic box of 125 fully flexible CH_2Cl_2 solvent molecules, which allowed us to examine the time-dependent energy in the HCN normal modes and the cyclohexyl co-product in more detail than was experimentally possible. Initially, we performed the following two sets of classical dynamics simulations: (i) 250 non-reactive microcanonical trajectories in which we investigated the relaxation of vibrationally excited HCN(001) in neat CH_2Cl_2 solvent, and (ii) 250 reactive trajectories using a recently developed analytic reactive force field for $CN + c\text{-}C_6H_{12} \rightarrow HCN + c\text{-}C_6H_{11}$ in CH_2Cl_2[15]. For each trajectory, the number of particles (N), volume (V) and energy (E) were conserved. Time-dependent C–H stretch normal mode energies, $E_{CH}(t)$, were obtained by projecting the molecular Cartesian coordinates and momenta into the normal mode frame of molecular equilibrium geometries. The results were then averaged over all 250 trajectories to obtain ensemble averaged energies, $\overline{E_{CH}}(t)$, which are shown in Fig. 3.

Figure 3 indicates that the $\overline{E_{CH}}(t)$ decay in neat CH_2Cl_2 may be fit using a single exponential with a time constant of 736 ± 531 ps^{-1}. In marked contrast, the $\overline{E_{CH}}(t)$ profile obtained when HCN is formed via reaction (R1) shows multiple decay timescales—with a fast initial

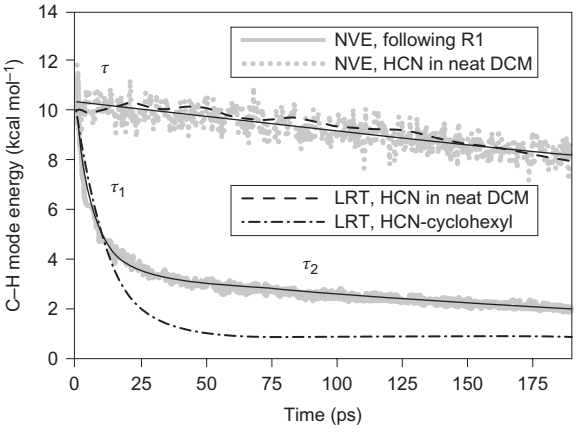

Figure 3 | Time-dependence of the HCN C–H stretching energy obtained from averaging over 250 non-equilibrium MD simulations. The simulations were carried out in (i) neat dichloromethane (DCM) solvent (solid black line fit to a single exponential decay curve with time constant τ); (ii) following abstraction of an H atom from *c*-C_6H_{12} in DCM solvent (solid black line fit to a biexponential decay curve with time constants τ_1 and τ_2). Also shown are the LRT predictions obtained from a single equilibrium trajectory of HCN relaxation in (i) neat DCM and (ii) locked with *c*-C_6H_{11} in a DCM solvent cage. This figure shows that HCN relaxation following reaction (R1) occurs on two different LRT timescales.

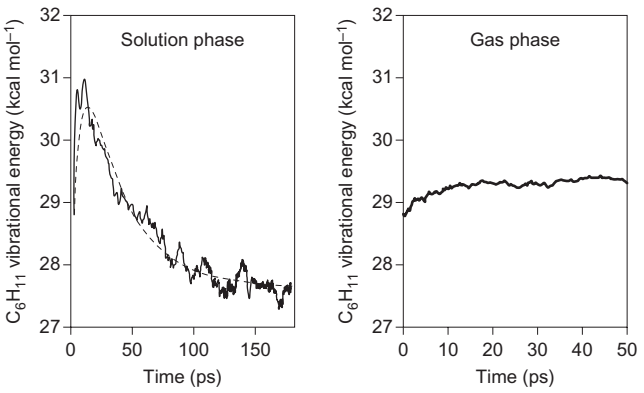

Figure 4 | Comparison of the total vibrational energy of the nascent *c*-C_6H_{11} in both gas-phase and solution-phase reactive dynamics simulations. The solution-phase panel shows the fit (dashed line) obtained using the simple energy flow kinetic model described in the text. This figure demonstrates that, following reaction (R1), the fast HCN relaxation reflects rapid energy exchange with its radical co-product.

decay and a slower long time decay. Fitting these data with a biexponential gives a fast decay time constant τ_1 of 7.0 ± 0.2 ps, and a slow time constant τ_2 of 204 ± 33 ps. The latter is close to the value of 144 ± 8 ps obtained from experimental infrared pump–probe measurements of HCN (001) decay in a CH_2Cl_2 solvent and 1 M *c*-C_6H_{12} (ref. 16).

The results of the simulations discussed above were compared to the predictions of time-independent LRT in both the presence and absence of *c*-C_6H_{11}. For this purpose, we performed two different classical dynamics simulations: (i) a single 2 ns microcanonical simulation of HCN in CH_2Cl_2 and (ii) a single 2 ns microcanonical simulation in CH_2Cl_2 where we turned off diffusion and used the AXD algorithm[17,18] to constrain the HCN and *c*-C_6H_{11} to have a centre-of-mass separation less than 5.7 Å. In each case, the initial coordinates and momenta were obtained by sampling a 298 K ensemble, and subsequent correlation functions of E_{CH}, $C(t)$, were calculated as:

$$C(t) = \langle E_{CH}(t_0)E_{CH}(t_0 + t)\rangle - \langle E_{CH}\rangle^2 \tag{1a}$$

where the angle brackets denote averaging over the whole trajectory, so that, for example, $\langle E_{CH}\rangle$ is the average time-independent C–H stretching energy at thermal equilibrium, and t_0 represents all possible start times within the trajectory. The LRT prediction was calculated, using $C(t)$, as:

$$\frac{\overline{E_{CH}}(t) - \langle E_{CH}\rangle}{\overline{E_{CH}}(0) - \langle E_{CH}\rangle} = \frac{C(t)}{C(0)} \tag{1b}$$

As shown in Fig. 3, the time-dependent energy profiles of excited HCN in neat CH_2Cl_2 averaged over 250 trajectories decay in close agreement with single trajectory predictions based on LRT calculated from equation (1b), showing that an excitation of 10 kcal mol^{-1} is not so large a perturbation as to make the CH response nonlinear.

Figure 3 shows that neither of the HCN LRT correlation functions (either in bulk solvent or locked with *c*-C_6H_{11} in a solvent cage) fully explains the observed decay trace following (R1). At short times, linear response theory for HCN and cyclohexyl locked within a solvent cage correctly captures the physics, whereas at longer times, the decay approaches the LRT predictions for HCN decay in neat CH_2Cl_2. The question that arises is as follows. Why is there such an apparently strong violation of simple LRT for relaxation of the CH mode when HCN is formed in reaction (R1) and, specifically, why is the energy relaxation at short times following reaction so much faster than at longer times?

The answer lies in recognizing that we must not only consider energy deposition in the nascent HCN formed in reaction (R1), but also in its *c*-C_6H_{11} co-product. Accordingly, we used the normal mode projection algorithm described above to examine $\overline{E_{C_6H_{11}}}(t)$, the time dependent vibrational energy content of *c*-C_6H_{11} following its formation in reaction (R1). The results averaged over 250 reactive trajectories in both the gas phase and in CH_2Cl_2 solvent are shown in Fig. 4.

Whereas $\overline{E_{C_6H_{11}}}(t)$ is more or less constant with time in gas-phase simulations (Fig. 4, right panel), it shows a significantly different energy profile in the solution-phase dynamics (left panel), with a rise at short times followed by a subsequent decay. The profile of $\overline{E_{C_6H_{11}}}(t)$ following reaction (R1) may be reasonably well described by the following simple irreversible kinetic scheme, which maps the flow of excess vibrational energy between HCN, *c*-C_6H_{11} and the CH_2Cl_2 solvent bath:

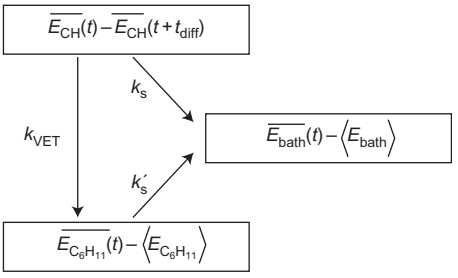

where k_{VET} is the rate coefficient for flow of excess CH stretching vibrational energy, $\overline{E_{CH}}$, from HCN to *c*-C_6H_{11}, k_s is the rate coefficient for flow of CH stretch energy in HCN to the CH_2Cl_2 solvent bath in the presence of *c*-C_6H_{11}, k'_s is the rate coefficient for energy flow from vibrationally excited *c*-C_6H_{11} to the solvent bath in the presence of HCN, and t_{diff} is the time at which the HCN has diffused far enough away from *c*-C_6H_{11} that the k_{VET} and k_s pathways effectively shut off. Energy transfer from HCN to solvent in the absence of *c*-C_6H_{11}, as shown in Fig. 3, is slow enough to be neglected at times smaller than t_{diff}. The rate equations that make up the kinetic mechanism for mapping energy flow in the immediate wake of reaction (R1) may be solved using an integrating factor to give an analytic solution for the ensemble-averaged time-dependent energy in *c*-C_6H_{11}:

$$\begin{aligned}
&\overline{E_{C_6H_{11}}}(t) = A\exp[-(k_{VET} + k_s)t] + B\exp(-k_{VET}t) + E_{C_6H_{11}}(\infty)\\
&A = \frac{k_{VET}\left(\overline{E_{CH}}(0) - \overline{E_{CH}}(t_{diff})\right)}{k'_s - k_{VET} - k_s}\\
&B = \overline{E_{C_6H_{11}}}(0) - \langle E_{C_6H_{11}}\rangle - A
\end{aligned} \tag{2}$$

The left panel of Fig. 4 shows fits obtained using equation (2) with the following constraints: (i) $k_{VET} + k_s$ is equal to $1/\tau_1$ (where τ_1, shown in Fig. 3, is the time constant for energy decay from the nascent HCN following abstraction), and (ii) the average initial

Table 1 | Parameters obtained from fitting the Fig. 4 data using equation (2).

Parameter	Value
k_{VET}	0.076 ps^{-1}
k_s	0.067 ps^{-1}
k'_s	0.030 ps^{-1}
$\overline{E_{CH}}(0) - \overline{E_{CH}}(t_{diff})$	6.0 kcal mol^{-1}
$\langle E_{C_6H_{11}}\rangle$	27.6 kcal mol^{-1}

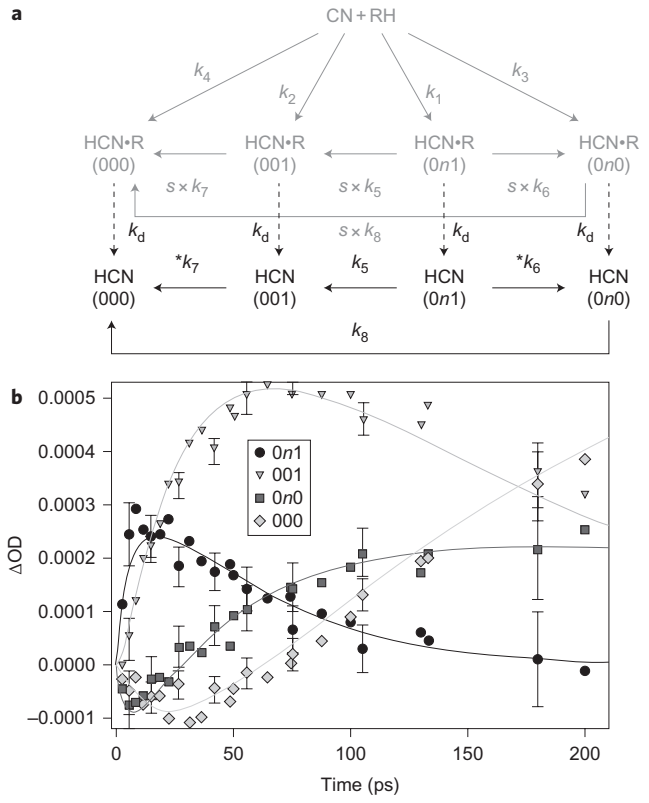

Figure 5 | Kinetic model demonstrating improved agreement with experiments. a, This model accounts for the different LRT regimes that HCN experiences. Grey represents dynamics when the nascent HCN is complexed to R (c-C_6H_{11}) within the initial solvent cage, the dashed line represents diffusion of HCN away from R into the bulk solvent with rate coefficient k_d, and black represents subsequent relaxation kinetics of HCN in the bulk solvent. The asterisk denotes that the fit parameters were not floated, but fixed to experimental IR pump–probe measurements. **b**, Same data and errors as in Fig. 2b, with the difference that the solid lines now show the fit obtained using the dual-timescale LRT kinetic model in **a**. Compared to Fig. 2b, this figure shows the significantly improved agreement between model and observations at times less than 50 ps, where the HCN relaxation dynamics are dominated by in-cage relaxation processes in the vicinity of the c-C_6H_{11} co-product.

energy ($t = 0$) in the c-C_6H_{11} fragment is 28.8 kcal mol^{-1}. The parameters producing the fit are provided in Table 1.

The values of the rate coefficients in Table 1 show that the fast energy transfer from HCN to c-C_6H_{11} has a time constant of ~15 ps, during which time the relative separation between the HCN and c-C_6H_{11} centres of mass following reaction (R1) increases from an initial value of ~5 Å to ~6.3 Å. Another interesting fitting result is the fact that the rate coefficient for energy transfer from HCN to solvent in the presence of c-C_6H_{11}, k_s, is similar in value to k_{VET}. Although a reasonable, albeit much less accurate fit can be obtained by setting $k_s = 0$ (Supplementary Fig. S2), this suggests that c-C_6H_{11} serves two roles with respect to HCN energy relaxation within the solvent cage: it is an efficient acceptor of vibrational energy from HCN, and it also mediates efficient energy transfer from HCN to the CH_2Cl_2 solvent[19,20]. The difference between $\overline{E_{CH}}(0)$, which is ~10.5 kcal mol^{-1}, and $\overline{E_{CH}}(t_{diff})$ is ~6 kcal mol^{-1}, in reasonable agreement with extrapolation of the τ_2 decay in Fig. 3 to $t = 0$.

A microscopic picture of post-reaction energy transfer thus emerges. Immediately following reaction, the vibrational energy distributions in both HCN and c-C_6H_{11} are similar to their gas-phase values. At short times, energy relaxation of the nascent HCN is efficient given its proximity to c-C_6H_{11}, which soaks up vibrational energy from the HCN, and also facilitates energy transfer to the solvent. In this regime, the LRT correlation function obtained from turning off diffusion and locking HCN and cyclohexyl in a solvent cage gives a good representation of the dynamics. As the HCN and c-C_6H_{11} diffuse away from one another into the bulk solvent, HCN energy relaxation becomes less efficient, approaching the relaxation that would be expected on the basis of the LRT correlation functions obtained in neat CH_2Cl_2. In the wake of reaction (R1), the hot nascent HCN moves between the limits of these two linear response theory regimes.

Experimental observations of multiple relaxation regimes. Having established that the HCN decay follows multiple timescales and the corresponding inadequacy of a simple time-independent linear response theory treatment, we revisited the experimental data in Fig. 2b. A simple improvement of the kinetic model in Fig. 2a is shown in Fig. 5a. It incorporates the two different LRT regimes that the HCN experiences in the wake of reaction (R1). The first occurs when the nascent HCN undergoes efficient energy relaxation within a caged supermolecular post-reaction complex with c-C_6H_{11} (R in Fig. 5a). The second occurs when the supermolecular complex has undergone diffusional dissociation into the bulk solvent. The Fig. 5a model includes two parameters beyond those in Fig. 2a: (i) k_d, which is a rate coefficient representing diffusion from the solvent caged LRT regime to bulk solvent LRT regime, and (ii) s, which accounts for the fact that HCN energy relaxation locked with c-C_6H_{11} in a solvent cage is s times faster than in free CH_2Cl_2.

Using the kinetic model in Fig. 5a, we refit the experimental data using a numerical integration procedure. The fit is shown in Fig. 5b, and the floated average parameters obtained from fits carried out on different data sets are given in Table 2.

At long times, the results of fitting Fig. 5a to the time-resolved experimental data differ little from those obtained with Fig. 2a. The real improvement, shown in Fig. 5b, is that Fig. 5a provides a significantly better representation of the short-time HCN (000) and HCN (0n0) population inversions—an improvement that is exactly within the time domain where our previous time-independent LRT fitting procedure was most inadequate for describing HCN energy relaxation locked in a solvent cage with c-C_6H_{11}. The parameters in Table 2 indicate that the respective branching ratios for the pathways corresponding to k_1, k_2, k_3 and k_4 are 0.74, 0.16, 0.07 and 0.03, showing that reaction (R1) predominantly forms HCN with both bend and stretch excitation, in good agreement with detailed analyses of the energy deposition in HCN obtained from both gas- and solution-phase MD simulations[15]. The rate coefficient for diffusion of HCN away from c-C_6H_{11} in CH_2Cl_2, k_d, is compatible with experimental measurements of the self-diffusion coefficient of CH_2Cl_2 at 298 K (ref. 21). Over a time of $1/k_d$, the one-dimensional CH_2Cl_2 self-diffusion

Table 2 | Parameters obtained from average fits over a number of experimental data sets using Fig. 5a (errors are 95% confidence limits).

Parameter	Value
k_1	$(2.20 \pm 0.25) \times 10^{-2}$ ps^{-1}
k_2	$(4.56 \pm 0.69) \times 10^{-3}$ ps^{-1}
k_3	$(2.17 \pm 1.10) \times 10^{-3}$ ps^{-1}
k_4	$(9.86 \pm 0.83) \times 10^{-4}$ ps^{-1}
s	10.9 ± 1.7
k_d	$(8.89 \pm 2.86) \times 10^{-2}$ ps^{-1}
k_5	$(7.80 \pm 1.03) \times 10^{-3}$ ps^{-1}
k_8	$(3.64 \pm 0.67) \times 10^{-4}$ ps^{-1}

distance is on the order of 6 Å. The scaling factor s has a best fit value of 10.9 ± 1.7. Within error bars, this is within a factor of two of the value of 29.1 ± 4.8 suggested by the MD results in Fig. 3. This level of agreement is reasonable, considering the approximations we have made in treating the energy transfer process with classical mechanics the Merck mechanics, force field (MMFF).

Discussion

The combined theoretical and experimental work presented herein shows that ultrafast experimental observations of energy relaxation for HCN in the wake of a solution-phase bimolecular reaction occur on multiple timescales. There are two relevant LRT limits—one for a solvent caged HCN–cyclohexyl complex and one for HCN in bulk CH_2Cl_2. As HCN diffuses out of the solvent caged supermolecular co-product complex into the bulk, the structure of its effective liquid environment changes, and the initial energy transfer efficiency diminishes. For the reverse reaction, which has a much higher barrier, microscopic reversibility dictates that similar effects will occur in what would be a supermolecular reactant complex.

This work provides an exciting link between the results obtained from MD simulations, and what appear to be implicit experimental observations of ultrafast liquid structural dynamics. It sheds light on the microscopic origins and time dependence of energy transfer in chemical reactions, and suggests that (i) kinetic models derived from a simple time-independent LRT approach are not necessarily transferable to systems that feature atomic reaction dynamics, and more sophisticated treatments are required[9,22]; (ii) models that represent energy relaxation in terms of time-averaged collision frequencies and energy transfer probabilities[23,24], such as isolated binary collision models, may not be accurate in the limit of short times following (or before) a bimolecular or unimolecular dissociation reaction unless they are modified to account for changes in liquid structural dynamics; and (iii) energy transfer and subsequent chemical reactions that follow on from solution-phase bimolecular reactions and unimolecular dissociations in solution are sensitive to the lifetime of solvent caged supermolecular complexes, whose energy transfer properties may be significantly distinct from the bulk on ultrafast timescales.

Recently, Stratt and co-workers[5,10] have argued that the relaxation of rotationally excited CN to equilibrium following ICN photodissociation in an argon solvent is characterized by two different timescales. The origin of these timescales is related to the efficiency with which the rotationally hot CN is capable of perturbing the solvent structure. At very short times, when the argon is relatively unperturbed from its equilibrium structure, relaxation is fast and well-described by LRT. After the hot CN has locally perturbed the solvent structure by effectively carving out a solvent bubble in which it can rotate almost freely, relaxation is significantly slower. This work presents a sort of vibrational analogue to those observations, with HCN relaxation moving between two different regimes depending on the liquid structure in which it is embedded. The goodness of the biexponential fit in Fig. 3 suggests that the switching between LRT domains is relatively abrupt.

Sophisticated experimental and theoretical methods are increasingly revealing the details of time-resolved chemical dynamics in solution[19,20,25] to better understand how these impact mode-selective chemistry[26], biochemistry[27,28] and the outcomes of chemical reactions[29,30]. In that context, this work represents a step towards revealing fundamental microscopic details of condensed phase thermal reaction dynamics, and delineating appropriate regimes for applying models as widespread as LRT, especially given that the vibrational energies in our system are rather characteristic of typical thermal reaction energies encountered in a wide range of systems spanning synthetic and biochemistry.

Methods

Fully flexible classical MD simulations were run using a locally modified version of the CHARMM software suite. The reactive CN + cyclohexane potential was obtained by nonlinear least-squares fitting of an empirical valence bond model to CCSD(T) electronic structure theory calculations extrapolated to the infinite basis set limit. The diagonal elements of the Hamiltonian matrix were obtained using the Merck MMFF implementation in CHARMM. Off-diagonal elements were represented as Gaussians, the parameters of which were determined using the aforementioned fitting. Energy disposal in the nascent HCN was determined by projecting its kinetic energy and geometry into the 3N-5 Cartesian normal mode displacements of equilibrium HCN.

The MD simulations used a leapfrog Verlet integration scheme, with thermal equilibration runs followed by subsequent microcanonical trajectories. Batches of 250 solution-phase thermal equilibration runs lasted 200 ps (timestep, 0.5 fs), with a Langevin friction coefficient of 10 ps^{-1}. The subsequent microcanonical trajectories had a duration of 200 ps and used a 0.1 fs timestep. CN and C_6H_{12} were solvated within a 23.7 $Å^3$ periodic box filled with 125 molecules of CH_2Cl_2, corresponding to the experimental 298 K CH_2Cl_2 density of 1.33 g ml^{-1}. Reaction events were accelerated using the recently developed boxed molecular dynamics method[17,18]. Simulations of energy relaxation of HCN were carried out in the same way as detailed above, with the difference that $v \approx 1$ initial excitation was placed in the CH stretch. Further simulation details are available in a recent publication[15].

Received 7 June 2011; accepted 22 August 2011; published online 25 September 2011

References

1. Gruebele, M. & Wolynes, P. G. Vibrational energy flow and chemical reactions. *Acc. Chem. Res.* **37,** 261–267 (2004).
2. Stratt, R. M. Chemistry—nonlinear thinking about molecular energy transfer. *Science* **321,** 1789–1790 (2008).
3. Chandler, D. *Introduction to Modern Statistical Mechanics* (Oxford Univ. Press, 1987).
4. Turi, L., Minary, P. & Rossky, P. J. Non-linear response and hydrogen bond dynamics for electron solvation in methanol. *Chem. Phys. Lett.* **316,** 465–470 (2000).
5. Moskun, A. C., Jailaubekov, A. E., Bradforth, S. E., Tao, G. H. & Stratt, R. M. Rotational coherence and a sudden breakdown in linear response seen in room-temperature liquids. *Science* **311,** 1907–1911 (2006).
6. Bragg, A. E., Cavanagh, M. C. & Schwartz, B. J. Linear response breakdown in solvation dynamics induced by atomic electron-transfer reactions. *Science* **321,** 1817–1822 (2008).
7. Fonseca, T. & Ladanyi, B. M. Breakdown of linear response for solvation dynamics in methanol. *J. Phys. Chem.* **95,** 2116–2119 (1991).
8. Smallwood, C. J., Bosma, W. B., Larsen, R. E. & Schwartz, B. J. The role of electronic symmetry in charge-transfer-to-solvent reactions: quantum nonadiabatic computer simulation of photoexcited sodium anions. *J. Chem. Phys.* **119,** 11263–11277 (2003).
9. Geissler, P. L. & Chandler, D. Importance sampling and theory of nonequilibrium solvation dynamics in water. *J. Chem. Phys.* **113,** 9759–9765 (2000).
10. Tao, G. H. & Stratt, R. M. The molecular origins of nonlinear response in solute energy relaxation: the example of high-energy rotational relaxation. *J. Chem. Phys.* http://dx.doi.org/10.1063/1.2336780 (2006).
11. Bethardy, G. A., Northrup, F. J. & Macdonald, R. G. The initial vibrational level distribution and relaxation of HCN[$X^1\Sigma^+(v_1,0,v_3)$] in the CN ($X\ ^2\Sigma^+$) + $CH_4 \rightarrow HCN + CH_3$ reaction system. *J. Chem. Phys.* **105,** 4533–4549 (1996).
12. Bethardy, G. A., Northrup, F. J., He, G., Tokue, I. & Macdonald, R. G. Initial vibrational level distribution of HCN[$X\ ^1\Sigma^+(v_1 0 v_3)$] from the CN($X^2\Sigma^+$) + $H_2 \rightarrow HCN + H$ reaction. *J. Chem. Phys.* **109,** 4224–4236 (1998).
13. Bethardy, G. A., Northrup, F. J. & Macdonald, R. G. The initial vibrational state distribution of HCN $X\ ^1\Sigma^+(v_1,0,v_3)$ from the reaction CN($^2\Sigma^+$) + $C_2H_6 \rightarrow HCN + C_2H_5$. *J. Chem. Phys.* **102,** 7966–7982 (1995).
14. Bethardy, G. A., Wagner, A. F., Schatz, G. C. & terHorst, M. A. A quasiclassical trajectory study of product state distributions from the CN + $H_2 \rightarrow HCN + H$ reaction. *J. Chem. Phys.* **106,** 6001–6015 (1997).
15. Glowacki, D. R., Orr-Ewing, A. J. & Harvey, J. N. Product energy deposition of CN + alkane H abstraction reactions in gas and solution phases. *J. Chem. Phys.* **134,** 214508 (2011).
16. Greaves, S. J. *et al.* Vibrationally quantum-state-specific reaction dynamics of H atom abstraction by CN radical in solution. *Science* **331,** 1423–1426 (2011).
17. Glowacki, D. R., Paci, E. & Shalashilin, D. V. Boxed molecular dynamics: decorrelation timescales and the kinetic master equation. *J. Chem. Theory Comput.* **7,** 1244–1252 (2011).
18. Glowacki, D. R., Paci, E. & Shalashilin, D. V. Boxed molecular dynamics: a simple and general technique for accelerating rare event kinetics and mapping free energy in large molecular systems. *J. Phys. Chem. B* **113,** 16603–16611 (2009).

19. Owrutsky, J. C., Raftery, D. & Hochstrasser, R. M. Vibrational relaxation dynamics in solutions. *Annu. Rev. Phys. Chem.* **45,** 519–555 (1994).
20. Elles, C. G. & Crim, F. F. Connecting chemical dynamics in gases and liquids. *Annu. Rev. Phys. Chem.* **57,** 273–302 (2006).
21. Dang, L. X. Intermolecular interactions of liquid dichloromethane and equilibrium properties of liquid–vapor and liquid–liquid interfaces: a molecular dynamics study. *J. Chem. Phys.* **110,** 10113–10122 (1999).
22. Laird, B. B. & Thompson, W. H. On the connection between Gaussian statistics and excited-state linear response for time-dependent fluorescence. *J. Chem. Phys.* http://dx.doi.org/10.1063/1.2747237 (2007).
23. Harris, A. L., Brown, J. K. & Harris, C. B. The nature of simple photodissociation reactions in liquids on ultrafast timescales. *Annu. Rev. Phys. Chem.* **39,** 341–366 (1988).
24. Nandi, N., Bhattacharyya, K. & Bagchi, B. Dielectric relaxation and solvation dynamics of water in complex chemical and biological systems. *Chem. Rev.* **100,** 2013–2045 (2000).
25. Voth, G. A. & Hochstrasser, R. M. Transition state dynamics and relaxation processes in solutions: a frontier of physical chemistry. *J. Phys. Chem.* **100,** 13034–13049 (1996).
26. Crim, F. F. Chemical dynamics of vibrationally excited molecules: controlling reactions in gases and on surfaces. *Proc. Natl Acad. Sci. USA* **105,** 12654–12661 (2008).
27. Noé, F. *et al.* Dynamical fingerprints for probing individual relaxation processes in biomolecular dynamics with simulations and kinetic experiments. *Proc. Natl Acad. Sci. USA* http://dx.doi.org/10.1073/pnas.1004646108 (2011).
28. Franco, M. I., Turina, L., Mershin, A. & Skoulakisa, E. M. C. Molecular vibration-sensing component in *Drosophila melanogaster* olfaction. *Proc. Natl Acad. Sci. USA* http://dx.doi.org/10.1073/pnas.1012293108 (2011).
29. Glowacki, D. R., Liang, C. H., Marsden, S. P., Harvey, J. N. & Pilling, M. J. Alkene hydroboration: hot intermediates that react while they are cooling. *J. Am. Chem. Soc.* **132,** 13621–13623 (2010).
30. Goldman, L. M., Glowacki, D. R. & Carpenter, B. K. Nonstatistical dynamics in unlikely places: [1,5] hydrogen migration in chemically activated cyclopentadiene. *J. Am. Chem. Soc.* http://dx.doi.org/10.1021/ja1095717 (2011).

Acknowledgements

T.A.A. Oliver, M.N.R. Ashfold, I.P. Clark, G.P. Greetham, A.W. Parker and M. Towrie are thanked for their contributions to the experimental work. Funding was provided by the Engineering and Physical Sciences Research Council Programme (grant EP/G00224X). The authors thank the Leverhulme Trust for an Early Career Research Fellowship (S.J.G.) and the Royal Society and the Wolfson Foundation for a Research Merit Award (A.J.O.E).

Author contributions

D.R.G. and J.N.H. conceived and designed the simulations. D.R.G. wrote the simulation code, performed the simulations and analysed data. A.J.O.E. conceived the experimental study, and R.A.R, S.J.G. and A.J.O.E. obtained and analysed the experimental data and performed the initial kinetic modelling. D.R.G. wrote the manuscript, with comments and discussions from all the authors.

Additional information

The authors declare no competing financial interests. Supplementary information accompanies this paper at www.nature.com/naturechemistry. Reprints and permission information is available online at http://www.nature.com/reprints. Correspondence and requests for materials should be addressed to D.R.G. and J.N.H.